Atmospheric Smog Modeling Using ASTER Absorption Bands and Its Correlation with In-*situ* Ground Sensor *Data*

Parthasarathi Roy[*], J. O. Brumfield[*] and A. Vaseashta[**]

[*]Graduate Program in Physical Sciences, Marshall University
[**]Nanomaterials Processing & Characterization Laboratories
One John Marshall Drive, Huntington, WV, roy29@marshall.edu

ABSTRACT

The focus of this research investigation is to assess atmospheric pollutants and their spectral characteristic signatures by ASTER satellite sensor data and to find correlations with ground sensor observations. Principal Component Analysis (PCA), Density Slicing (DS), Band Ratioing (BR), and Band-pass filtering (BPF) techniques are applied to extract features in the ASTER datasets. Spectral signatures in graphical form of the atmospheric features are obtained and compared both in short wave infra-red (SWIR) and thermal infra-red (TIR) bands. Despite broader bandwidth of ASTER as compared to hyperspectral satellite systems, an excellent high correlation is observed in spectral response of all TIR bands and moderate correlation with SWIR bands of ASTER with ground sensor monitoring

Keywords: Smog, Absorption Bands, Satellite-Imagery, Spectral Signature, Sensors, ASTER.

1 INTRODUCTION

Atmospheric pollution was previously considered as a 'Brown Cloud' phenomenon restricted to industrialized urban regions. Studies in field stations and satellite observations made since the last decade revealed that brown cloud (haze or smog) phenomenon which is normally associated with urban regions now spans continents and ocean basins worldwide (Ramanathan and Ramanna, 2003). Anthropogenic activities are considered to be as the primary cause of pollution in the atmosphere. Gaseous air pollutants, like NO_x, SO_2 , CO, and CH_4 , are some of the primary air pollutants and secondary pollutants, like HNOx, HSOx and aldehydes, are created from the primary pollutants by complex photochemical reactions in the presence of ultra-violate (UV) radiation forming free radicals in the atmosphere (UNEP, 2005). Aerosols are complex mixture of chemical species consisting of organic and elemental carbon, mineral dust, sulfates, nitrates, dust and fly ash particles and sea salt and water vapor (Satheesh and Ramanathan (2001). Aerosols can be non-respirable (of size>10 μ m), respirable (PM_10 of size<10 μ m), or inhalable (PM_2.5 of size<2.5 μ m). Both of these aerosols are called "Particulate matters" (PM) have been shown to cause health effects but the latter (i.e. PM_2.5) are the most damaging because they can penetrate into much deeper parts of the respiratory tract, namely the alveolar regions of the lungs (WHO, 2000). Atmospheric aerosols affects the earth's energy budget directly by scattering and absorbing radiation and indirectly by acting as cloud condensation nuclei and, thereby, affecting cloud properties (Yu et al. 2005). The appearance of a pollution layer with more absorption and scattering of solar radiations, particularly long-wave infrared radiations, decreases the atmospheric transmission factor, and changes the radiation fluxes, not only at the ground surface, but also at the top of the atmosphere, thereby significantly perturbing the atmospheric absorption of solar radiation. These aerosol-induced changes in the radiation budget are referred to as 'radiative forcing'. A relatively small proportion of aerosols can play a dominant role not only from reduction in surface solar radiation but also from latent heat fluxes, atmospheric stability and the strength of convection currents (Menon et al 2002). There is observational evidence that aerosols can alter cloud properties (Lee et al. 2004). Spectral signatures of molecules particularly infrared (IR) absorption spectroscopy has played an important role in the identification of trace pollutants in both ambient air and synthetic smog systems. Molecular vibration and rotation causes absorption of radiation when the frequency of rotation and vibration are equal to frequency of solar radiation directed to the molecules. Spectral signatures of common atmospheric pollutants are collected from Jet Propulsion Laboratory (JPL)'s ASTER spectral Library, High-resolution Transmission Molecular Absorption (HITRAN) Database.

2 EXPERIMENTAL INVESTIGATIONS

Satellite image data consists of earth radiances observed by its sensors in different bands. For thermal infra-red (TIR) bands the radiances represent a function of the temperature, emissivity of the ground surface and the atmospheric column above and it's surrounding (ASTER Manual, NASA, 2000). Satellite image data can aid in detection, tracking and understanding of pollutant sources and transport by providing observations over large spatial domains, with three dimensional models (3-D Models). In most of the previous investigations of atmospheric Smog modeling, satellite images are used to extract air pollution by calculating optical thickness in, either visible spectral ranges or low spectral resolution short-wave infra red (SWIR) and thermal infra red (TIR) ranges (Schafer et. al , 2002). This research investigated three locations, where high pollution concentrations are reported by air quality monitoring agency and general media. Firstly San Francisco Bay area recorded CO and PM _10 concentration, exceeded federal standards, by 110% and 117% respectively

(South Coast Air Quality Management District, Annual Report, 2000). Secondly in Los Angeles County, Lynwood and Burbank's PM_10 concentration recorded in the year 2003, exceeded Federal standard for 30 days (California Air Resource Board report, 2003). Thirdly Charleston, West Virginia, is ranked as the sixteenth most polluted city (PM_2.5 species) in USA by the ALA 2005 report.

Advanced Spaceborne Thermal Emission and Reflection Radiometer **(ASTER)** is an imaging instrument flying on Terra satellite which was launched in December 1999 as part of NASA's Earth Observing System (EOS). Terra is orbiting the earth at 705 km altitude, in a sun-synchronous orbit. In ASTER sensor systems there are three visible and near infra-red (VNIR) bands has 15 m spatial resolution in 0.52 μm – 0.86 μm range, six SWIR bands has 30 m spatial resolutions in1.6 μm – 2.43 μm range, and five TIR bands has 90 m spatial resolution in 8.125 μm-11.65 μm range. ASTER raw level-1 (L1A) data of Los Angeles, San Francisco Bay Area, and Charleston, WV are acquired during fairly dry seasons and cloud free condition in order to accurately assess the atmospheric smog. Georegistered Digital Orthophoto Quarter-Quadrangles (DOQQ's) and ESRI shapefiles are used as base map. Air Quality Monitoring hourly data, on the same day as that of satellite data acquisition, and facilities emission data has been acquired and used in this research investigation.

Currently EPA monitoring stations use particle mass analysis instruments namely, Tapered Element Oscillating Microbalance (TEOM), Continuous Ambient Mass Monitor (CAMM), or Beta Attenuation Method Sampler (BAMS), (EPA and Air resources Board, 2005). The detection technologies employed in particle mass analysis instruments include Beta gauges, piezoelectric crystals and harmonic oscillating elements. These technologies were designed for real-time mass analysis of particles in size ranging up to 10 μm. Nanotechnology based sensors presents opportunities to create new and better products for orbital image and ground sensor initiatives. Nanotechnology based sensors are nanoparticles and nanotube based devices, where in some cases carbon nanotubes (CNTs) connect two metal electrodes and conductance between them is observed as a function of gate bias voltage (Vaseashta and Irudayaraj, 2005). Since electrical characteristics are influenced by the atomic structure, any change such as mechanical deformation and chemical doping, induce change in conductance, thus rendering such devices sensitive to their chemical and mechanical environment (Vaseashta and Irudayaraj, 2005) Nanotechnology offers the potential to improve exposure assessment by facilitating collection of a large number of measurements at a lower cost and improved specificity (Vaseashta et al, 2006).

ASTER L1A raw data, of the respective sites, has been geometrically corrected and geo-registered in Universal Transverse Mercator (UTM) coordinate system, and WGS84 datum, by image-to-image registration process with DOQQ in ER-Mapper 7.1 software. Principal Component Analysis (PCA) Technique has been applied to extract atmospheric smog in the imagery in ER-mapper 7.1 software. The PCA technique involves a mathematical procedure for simplifying a dataset by reducing multidimensional datasets to lower dimensions by analysis. It transforms a number of (possibly) correlated variables into a (smaller) number of uncorrelated variables called principal components (PC). Density slicing (DS) is a form of selective one-dimensional classification. The continuous pseudocolor scale of the resultant image is "sliced" into a series of classifications based on ranges of brightness values. DS technique has been applied on the resultant dataset in, band 14 for HNO_3 absorption band at 11 μm, band 7 for Carbon monoxide and carbonate absorption band at 2.3 μm. Band Ratioing (BR) is a process by which brightness values of satellite image pixels in one band are divided by the brightness values of their corresponding pixels in an another band in order to create an enhanced new output image, where subtle differences in spectral signatures are arequred (Jensen, 2005, Prentice Hall). High-pass filtering is a digital technique based on convolution process, applied in either the spatial or frequency domain. A high pass filter tends to retain the high frequency information within an image while reducing the low frequency information.

3 RESULTS AND DISCUSSION

GIS map of EPA monitoring stations (fig. 1a1) in San Francisco Bay area, Los Angeles (fig.1b1) and in Charleston (fig.1c1), created in ESRI ArcGIS 9.1 software, shows limited opportunity to assess air pollutant from in-situ air quality and facilities data provided by EPA. PCA image bands 1-14 of San Francisco Bay (fig. 1a2) shows; cloud pattern in different tones of blue in bands 1-9 (fig. 1a3) does not show different tones in pink. Similarly in Los Angeles the PCA image in bands 1-14, shows , cloud pattern in different tone in blue(fig. 1b2), but that in bands 1-9 does not show different tones in blue (fig. 1b3). However in Charleston PCA image in both sets of bands (fig. 1c2 and 1c3), shows different tones of cloud patterns.

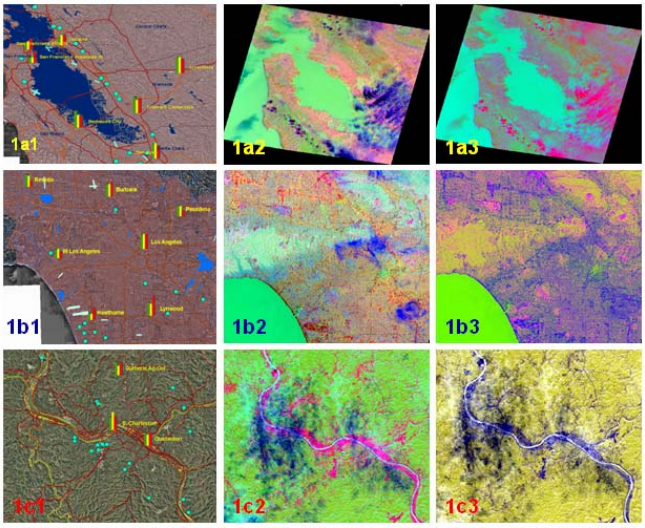

Figure 1: (1) *GIS map of industries location and EPA Air quality Monitoring Pollutant concentrations measured at the same time on the day of satellite data in (a1) San Francisco, (b1) Los Angeles and (c1) Charleston. Concentrations of CO*

NSTI-Nanotech 2007, www.nsti.org, ISBN 1420061836 Vol. 2, 2007

are shown in green, NOx in yellow, PM_10 in red bar graphs. (2) PCA ASTER processed images in band 14: (a2) San Francisco, (b2) Los Angeles and (c2) Charleston. (3) PCA ASTER processed images in band 7: (a3) San Francisco, (b3) Los Angeles and (c3) Charleston.

DS image of San Francisco bay area (fig. 2a1 and 2a2) in pseudo color with DOQQ as intensity layer displays different tones of brown, due to absorption in band 14 (HNO_3 absorption band) (fig. 2a1), but in band 7 (carbonates absorption band), the cloud patterns (fig. 2a2) do not show different tones in blues very clearly. Similarly in Los Angeles DS image in band 14 (fig. 2b1) shows air pollutants in different tones of blue, but DS image in band 7 (fig. 2b2) does not show air pollutants. Both of the DS images of Charleston (fig. 2c1 and 2c2) shows different tones of brown. Spectral signatures of air pollutants, in all SWIR bands 4-9, and all TIR bands 10-14, are detected by a traverse technique (Roy et. al., 2006) in ER-Mapper 7.1. Spectral signature of Berkeley area in San Francisco Bay ASTER image in SWIR (fig. 2a3) shows that the ASTER band 7 behaves abnormally compared to other bands, whereas the ASTER TIR bands 10-14 (fig. 2a4) shows almost similar behavior except bands 10 (9.0 μm) and 14 (11.0 μm) where more absorption is observed. Spectral signature of Los Angeles in SWIR bands (fig.2b3) shows that bands 9 and 5 behaves differently than other SWIR bands, but strong absorption in all TIR bands (fig. 2b4). In Charleston spectral signature images, SWIR bands 5, 7, 8 shows little variations (fig. 2c3), and TIR bands 13 and 14 shows much absorption and variations (fig. 2c4).

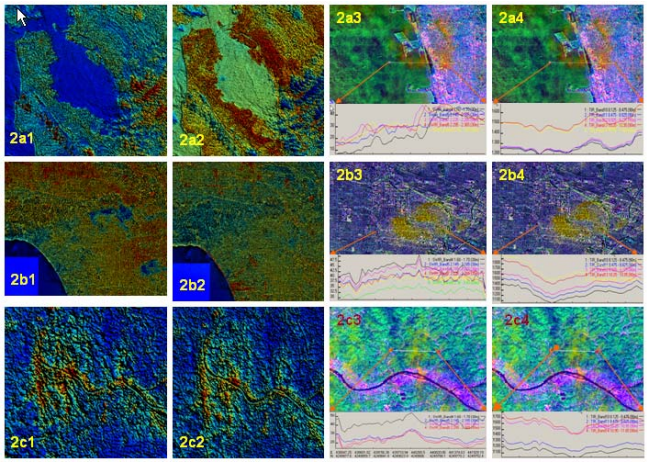

Figure 2: *Density sliced ASTER images (1) in band 14 and (2) band 7: (a1 and a2) San Francisco Bay area, (b1 and b2) Los Angeles, (c1 and2) Charleston. Spectral signatures compared in (3) SWIR bands (4) TIR bands: (a3 and a4) Berkeley, in San Francisco Bay area, (b3 and b4) Los Angeles, (c3 and c4) Charleston.*

In view of observed slight differences in spectral signatures in band 7, a band ratio image composite is created with red band ratioed as 14/10 , green band ratioed as 3/5 and blue band ratioed as 3/2. The resultant image of San Francisco (fig. 3a1) clearly distinguishes regular cloud patterns with atmospheric pollutants in different tones of red and brown. BR image of Los Angeles unable to distinguish any cloud pattern with plume (fig. 3b1), whereas the BR image of Charleston clearly shows different tones of cloud mask in yellow (fig. 3c1) in the imagery.

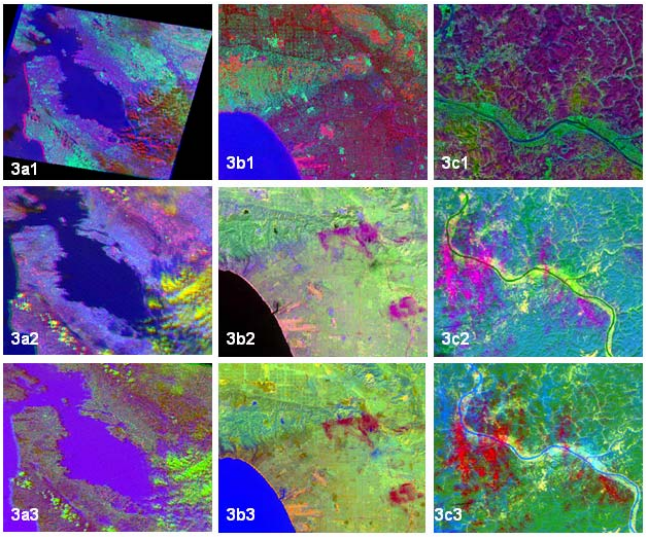

Figure 3: *(1)* ***Band ratio*** *composite image in RGB bands 3/2, 7/5, 14/10: (a1) San Francisco Bay (b1) Los Angeles area (c1) Charleston.* ***Band pass filtering*** *ASTER digital numbers in band 14, 7, and 3 – (2) Without High band-pass filter, (3) With High pass band filter, with: (a2 and a3) San Francisco. (b2 and b3) Los Angeles, (c2 and c31) Charleston.*

Spatial filtering technique is applied with band pixel digital numbers to enhance high frequency local variations. A convolution mask of 3x3 kernel size has been used with a center value as the digital number of the pixel in TIR band 14, SWIR band7, and VNIR band 3 in all the image data set. The images without filtering and after the filter is applied are shown in Figures 3a2, a3 for San Francisco), figures 3b2, b3 (for Los Angeles), and figures 3c2, c3 (for Charleston). In Bay area filtered image (fig. 3a2) differences in plume and cloud pattern are clearly distinguishable. In Los Angeles image before filtering (fig. 3b2) does not show pollution patterns over West Los Angeles. It shows only in Lynwood area and Los Angeles downtown area. The filtered image (fig. 3b3) shows plume patterns there. In Charleston different tones of cloud pattern (fig. 3c3) are highlighted in the filtered image.

Analysis of variance, or ANOVA, refers to partitioning the variation in a variable's values into variation among several groups or classes of observations. Statistical procedure, ANOVA by a 'general linear model' called 'PROC GLM' (general linear model) has been used in this research. All pixel values and pollutants concentrations levels are fed into PROC-GLM program in 'SAS' software, and a linear relationship is established. The interactions (Pollutant * City) were tested, with all SWIR and TIR bands. Results from PROC GLM program are shown in the Table-1. It is observed that there is significant city effect, which the results are not consistent among the cities. In SWIR bands ASTER Channels 5 – 9 (Table1) shows no correlation with PM_10 concentrations, but channel 7 was found weakly correlated with CO

concentrations. In TIR bands, ASTER channel 10-14, the relationship between spectral values and CO or NO_X were highly significant.

Table-1: *Probability error level of in ASTER reflectance value in correspond to the EPA pollutants monitoring of CO, NOx and PM_10 and respective cities (from 'ANOVA' ProcGLM, Program in SAS software. This table contains p-values; ns – non-significant if p>0.05.*

	ASTER Channels									
Source	5	6	7	8	9	10	11	12	13	14
CO	ns	ns	.0192	ns	ns	.0004	.0003	.0005	.0005	.0003
City	.0039	.0036	.0007	.0094	.0131	ns	.0177	.0019	.0013	.0001
NOx	.009	.0044	.0007	.0041	.0032	.0001	.0001	.0001	.0001	.0001
City	ns	ns	ns	ns	ns	.0015	.0024	.0007	.0002	.0001
PM_10	ns	ns	ns	ns	ns	.0164	.0193	.0466	.0332	.0236
City	.0133	.0057	.0098	.0293	.0233	.0296	.0147	.0071	.0044	.001

Scatter plots of Pollutant concentration with ASTER pixel digital data numbers are created for, CO, NOx and PM_10 of in bands 7 and 14 (fig. 4) suggests a city wise regional shifts in correlation of data swarm. For CO in band 7 Los Angeles and San Francisco Bay area are weakly correlated (fig.4a1). In band 14 shows a high correlation in San Francisco area, but a very weak negative correlation for Los Angeles and Charleston (fig. 4a2). For NOx in band 7 San Francisco and Charleston are highly correlated (fig. 4b1), but in Los Angeles very weak correlation is observed. NOx in band 14, Los Angeles and San Francisco are negatively correlated (fig. 4b2). PM_10 for band 10, in all the three sites, are not correlated (fig. 4c1). PM_10 for band 14 (fig. 4c2) low correlations is observed.

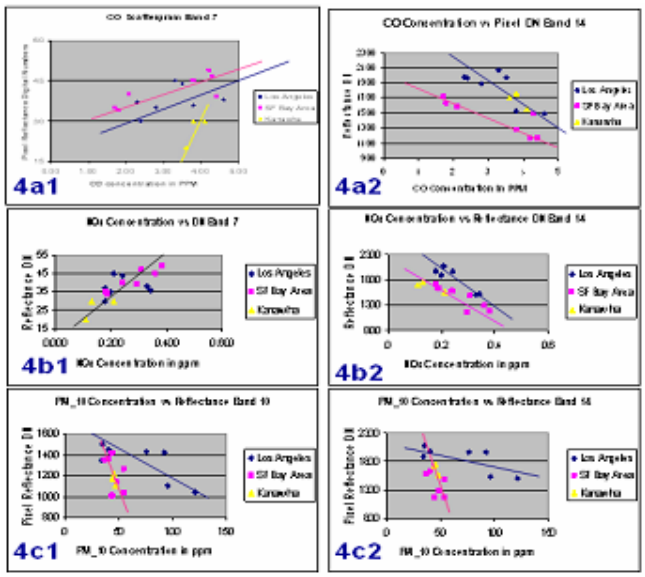

Figure 4: Scatter plot of EPA pollutant Concentration level at all the three sites against ASTER DN: (a1) and (a2) CO in band 7 and 14 respectively. (b1) and (b2) NOx in bands 7 and 14 respectively, (c1) and (c2) PM_10 in bands 7 and 14 respectively.

4. CONCLUSION

This research investigation presents a methodology to assess atmospheric pollution from a multi-spectral satellite platform. Statistical analysis support different feature extraction patterns of different kinds of air pollutants in the atmosphere of San Francisco, Los Angeles and Charleston. Future research investigations will focus on hyperspectral studies in order to find the subtle differences in spectral signature of atmospheric constituents and pollutants patterns using feature extraction and pattern recognition techniques in satellite sensor image systems and highly sensitive nanotechnology based ground sensors.

REFERENCES

[1] http://www.ats.ucla.edu/STAT/sas/library/repeated_ut.htm

[2] EPA Air Resources Board: State and Local Monitoring Network Report manual, October 2005.

[3] HITRAN : High-resolution Transmission Molecular Absorption database, see www.hitran.com

[4] Jensen, J. R.: Introductory Digital Image Processing: A Remote Sensing Perspective, Prentice Hall, 2005.

[5] Menon Surabi, James Hansen, Larissa Nazarenko, and Yunfeng Luo: Climate effects of Black Carbon Aerosols in China and India, Sciencemag.org, Vol-297, September 27, 2002.

[6] Petaja T., Kerminen V.M, Hameri K, Vaattovaara P: Effects of SO2 Oxidation on ambient aerosol growth in water and ethanol vapors: Atmospheric Chemistry and Physics-5, p- 767-779, 2005

[7] Ramanathan, V. Satheesh, S.K. Large Differences in Tropical Aerosol Forcing at the Top of the Atmosphere and Earth's Surface, Nature, 405, 60, 2001.

[8] Roy, P., J.O. Brumfield, A. Vaseashta: Smog Extraction in Urban Area using ASTER and its Correlation with In-situ Data, International Nanotechnology Congress, Nov. 2nd, 2006, International Association of Nanotechnology: See www.ianano.org

[9] UNEP: Atmospheric Brown Clouds, 2005 under the sponsorship of the United Nations Environmental Program and NOAA. See http://www.sianbrowncloud.ucsd.edu/.

[10] Vaseashta, A. and J. Irudayaraj : Nanostructured and Nanoscale Devices and Sensors, Journal of Optoelectronics & Advanced Materials Vol. 7, No. 1, p. 35-42, 2005.

[11] Vaseashta et al. Nanostructured and Advanced Materials for Applications in Sensor, Optoelectronic and Photovoltaic Technology, Springer (2005).

[12] Vaseashta, A., J.O. Brumfield, S.B. Vaseashta, J. Barrios, and P. Roy: Atmospheric Parameters Sensing Using Nanotechnology Based Sensors and Image Processed Real-Time Satellite Data, at Kassing et al. (eds.), Functional Properties of Nanostructured Materials, p- 443-448, Springer, Netherlands, 2006.

[13] WHO, 2000, Guidelines for Air Quality, World Health Organization Report, Geneva, 2000.

[14] Yu H. Y.J. Kaufman, M. Chin, G. Feingold, M. Zhou : A Review of Measurement-based Assessment of Aerosol Direct Radiative Effect and Forcing, Atmospheric Chemistry and Physics, May 2005.